Role of metabolic gases in bubble formation during hypobaric exposures

PHILIP P. FOSTER,[1] JOHNNY CONKIN,[1] MICHAEL R. POWELL,[2]
JAMES M. WALIGORA,[2] AND RAJ S. CHHIKARA[3]
[1]*Universities Space Research Association, Division of Space Life Sciences,* [2]*Environmental Physiology Laboratory, Life Sciences Research Laboratories, National Aeronautics and Space Administration Johnson Space Center, and* [3]*Division of Computing and Mathematics, University of Houston—Clear Lake, Houston, Texas, 77058*

Foster, Philip P., Johnny Conkin, Michael R. Powell, James M. Waligora, and Raj S. Chhikara. Role of metabolic gases in bubble formation during hypobaric exposures. *J. Appl. Physiol.* 84(3): 1088–1095, 1998.—Our hypothesis is that metabolic gases play a role in the initial explosive growth phase of bubble formation during hypobaric exposures. Models that account for optimal internal tensions of dissolved gases to predict the probability of occurrence of venous gas emboli were statistically fitted to 426 hypobaric exposures from National Aeronautics and Space Administration tests. The presence of venous gas emboli in the pulmonary artery was detected with an ultrasound Doppler detector. The model fit and parameter estimation were done by using the statistical method of maximum likelihood. The analysis results were as follows. *1*) For the model without an input of noninert dissolved gas tissue tension, the log likelihood (in absolute value) was 255.01. *2*) When an additional parameter was added to the model to account for the dissolved noninert gas tissue tension, the log likelihood was 251.70. The significance of the additional parameter was established based on the likelihood ratio test ($P < 0.012$). *3*) The parameter estimate for the dissolved noninert gas tissue tension participating in bubble formation was 19.1 kPa (143 mmHg). *4*) The additional gas tissue tension, supposedly due to noninert gases, did not show an exponential decay as a function of time during denitrogenation, but it remained constant. *5*) The positive sign for this parameter term in the model is characteristic of an outward radial pressure of gases in the bubble. This analysis suggests that dissolved gases other than N_2 in tissues may facilitate the initial explosive bubble-growth phase.

bubble growth; Doppler ultrasound; inert and noninert dissolved gases; tissue ratio; logistic model; log likelihood; gas kinetics

REDUCTION IN AMBIENT PRESSURE is experienced by divers, aviators, and astronauts. The Shuttle and the Russian Space Station Mir atmospheres are at a pressure of 101.3 kPa, but astronauts or cosmonauts are exposed to a reduced absolute pressure in the space suit when they are performing extravehicular activity (EVA). Decompression may lead to the formation and growth of gas bubbles within tissues (3, 4, 16), with a resultant risk of decompression illness (DCI). In humans, the composition of gas bubbles in tissues is not amenable to direct experimental verification. Furthermore, analysis of intravascular bubbles does not provide information about the fractions of dissolved gas in tissues participating in bubble formation (8). O_2 and CO_2 rapidly permeate in and out of the bubbles, compared with N_2 (13). After sufficient time, the gas in bubbles presumably equilibrates with metabolic levels of O_2 and CO_2 in mixed venous blood or tissue, and with the body saturation level for water vapor pressure (8, 13). In contrast to hyperbaric decompressions, metabolic gases form a large fraction of the gas in bubbles during hypobaric decompressions (15). Moreover, theoretical simulations utilizing a system of mathematical equations (13) suggested a significant role for metabolic gases in bubbles during hypobaric decompressions.

Our hypothesis is that metabolic gases are involved in the initial growth phase of bubbles. An analysis is made by using experimental results from human exposures conducted in altitude chambers that simulate EVA procedures. Oftentimes, venous gas emboli (VGE) can be detected in the venous blood flow (7, 9) when a Doppler ultrasound bubble detector is used. Bubbles spawned in capillaries of tissues were mobilized into the venous return by flexing the limb during the period of bubble monitoring. Models that account for the tensions of dissolved gases in tissues and predict VGE incidence were statistically fitted to the data. We evaluated whether the incorporation of an additional mechanistic parameter into a model produced a better fit to the observed response. The model with the best fit to the data is assumed to support the more realistic hypothesis.

METHODS

Glossary

$F_{I_{O_2}}$	Fraction of inspired O_2, dimensionless
$F_{I_{N_2}}$	Fraction of inspired N_2, dimensionless
i	Subscript for the ith record (426 records)
L	Likelihood function, dimensionless
LL	Natural logarithm of the likelihood function, dimensionless
$P_{A_{CO_2}}$	Alveolar CO_2 partial pressure of 5.33 kPa (40 mmHg)

$P_{A_{H_2O}}$ Alveolar H_2O pressure of 6.27 kPa (47 mmHg)
$P_{A_{N_2}}$ Alveolar N_2 partial pressure, kPa
Pa_{N_2} Arterial N_2 tension, kPa
$P_{A_{O_2}}$ Alveolar O_2 partial pressure, kPa
P_B Total absolute pressure of the breathing medium; pressure at altitude, kPa
P_{other} Additional dissolved gas tissue tension, kPa
P Probability of occurrence of VGE, dimensionless
$Pti_{N_2}(0)$ Initial N_2 tissue tension just before the procedure of interest, kPa
$Pti_{N_2}(t)$ Dissolved N_2 tissue tension at a time t; estimated dissolved N_2 tissue tension at the end of denitrogenation, kPa
R Respiratory exchange ratio, $\dot{V}_{CO_2}/\dot{V}_{O_2}$, dimensionless
$t_{1/2}$ Tissue half time for washin and washout of N_2, min
t Time of interest, usually the end of the O_2 prebreathing, min
$\dot{V}_{CO_2}$ Amount of CO_2 eliminated, l/min
$\dot{V}_{O_2}$ Rate of O_2 uptake, l/min
y_i VGE outcome, 1 if VGE occurred, or 0 if none, dimensionless

Estimation of Dissolved N_2 Tension in Tissues

The $P_{A_{N_2}}$ determines the Pa_{N_2}, and this in turn defines the dissolved N_2 tension in the tissues. The denitrogenation, or N_2 "washout" during the prebreathe procedure, consists of breathing an O_2-enriched breathing medium (2); this can be pure O_2 or an O_2-N_2 mixture with different inspired fractions of O_2 and N_2, denoted by $F_{I_{O_2}}$ and $F_{I_{N_2}}$, respectively. The $P_{A_{O_2}}$ is calculated by using the alveolar gas equation (10). The $P_{A_{N_2}}$ equals the total ambient pressure P_B of the breathing medium minus $P_{A_{CO_2}}$, $P_{A_{O_2}}$, and $P_{A_{H_2O}}$. In accordance with Dalton's law, the $P_{A_{N_2}}$ can be expressed as follows

$$P_{A_{N_2}} = P_B - (P_{A_{H_2O}} + P_{A_{CO_2}}) - (P_B - P_{A_{H_2O}})F_{I_{O_2}} + P_{A_{CO_2}} \times \left[F_{I_{O_2}} + \frac{(1 - F_{I_{O_2}})}{R}\right] \quad (1)$$

where alveolar partial pressures of gases ($P_{A_{O_2}}$, $P_{A_{CO_2}}$, and $P_{A_{N_2}}$) are under body conditions of temperature, ambient pressure, and saturation with water vapor (BTPS). Arterial O_2, CO_2, and N_2 tensions (Pa_{O_2}, Pa_{CO_2}, and Pa_{N_2}, respectively) are assumed to be equal to their alveolar partial pressures (e.g., $Pa_{N_2} = P_{A_{N_2}}$). To determine the influence of the respiratory exchange ratio R, we statistically optimized the value of R in the physiological range between 0.7 and 1.0.

Assuming a perfusion-limited system (2–4), an approximation of the N_2 partial tension of dissolved inert gas in the tissue during any N_2 partial pressure change in the breathing medium is provided by the classic exponential model

$$Pti_{N_2}(t) = Pa_{N_2} + [Pti_{N_2}(0) - Pa_{N_2}]e^{-[\ln(2)/t_{1/2}]t} \quad (2)$$

where ln (2) is the natural logarithm of 2 and t is the elapsed O_2 prebreathe time. The dissolved N_2 tissue tension at the end of each denitrogenation stage was estimated by using iterations with *Eq. 2* for each National Aeronautics and Space Administration (NASA) pre-EVA denitrogenation. MATHEMATICA software, version 2.2 (24), was employed for this purpose. The ascent time for each pressure change was included as part of the denitrogenation time.

NASA Hypobaric Data Set

Subjects. There were 164 volunteers (37 women and 127 men), who participated in 426 hypobaric exposures at the Johnson Space Center between 1982 and 1990. The average age was 31.38 ± 7.2 yr. Their individual characteristics were representative of the astronaut population. Women were included during the latter part of these studies. All were required to pass the United States Air Force Class III Flight Physical examination. The subjects signed an informed consent and were free to withdraw from the tests at any time.

Test procedures for simulated EVAs. The chamber tests were not all the same, since *1*) denitrogenation periods varied; *2*) the breathing gas during the denitrogenation was 100% O_2 at 101.3 kPa [14.7 lb./in.^{2} absolute (psia)]; *3*) however, some tests used a staged decompression, a prolonged stay at an atmosphere of 70.3 kPa (10.2 psia) enriched with O_2 and with a reduced N_2 partial pressure (26% O_2-74% N_2), as part of the denitrogenation process; *4*) at altitude, after the final decompression, the breathing gas was 100% O_2 or O_2-N_2 mixtures; *5*) the pressure at altitude ranged from 29.64 kPa (4.3 psia) to 44.80 kPa (6.5 psia); and *6*) the time at altitude varied from 3 to 6 h. In all these tests, no exercise was performed during the O_2 prebreathe, and subjects were reclined or seated. Each subject was exposed to a particular denitrogenation and decompression profile; several of the same profiles constituted a test. Twenty tests were conducted. When test groups were separated with respect to gender, the total number of groups was 23. A low level of exercise during the simulated EVA involving upper limbs with an average metabolic rate of 837 kJ/h (200 kcal/h) was performed.

Dependent variable. VGE in the pulmonary artery were detected with a Doppler ultrasound bubble detector in the precordial position at ~15-min intervals throughout the exposure. The bubbles were mobilized by flexing the joints and straining the muscle groups of a limb (1) at the time of bubble monitoring. It is assumed that we measure the "limb bubble-formation tendency" before the time of monitoring. We code the presence of VGE in the pulmonary artery as 1, or 0 if no bubbles were detected.

Independent variable. We define a dose for the decompression (2, 14) as tissue ratio (TR), which is the ratio of the calculated dissolved N_2 tissue tension for a given tissue to the ambient pressure

$$\text{Dose} = \text{TR} = \frac{Pti_{N_2}(t)}{P_B} \quad (3)$$

where $Pti_{N_2}(t)$ is the dissolved N_2 tissue tension at the end of the denitrogenation period, as obtained from *Eq. 2*, and P_B is the ambient pressure at altitude. In *Eq. 3*, TR is expressed by using only the calculated dissolved N_2 tissue tension. A second determination of dose, i.e., TR′, is considered to be

$$\text{Dose} = \text{TR}' = \frac{Pti_{N_2}(t) + P_{other}}{P_B} \quad (4)$$

where P_{other} is the magnitude of dissolved gas tissue tensions other than N_2. The addition of P_{other} tests whether dissolved gas tissue tension other than N_2 plays a significant role in bubble formation during hypobaric exposures.

Statistical Analysis

Logistic regression model. The probability of VGE occurrence is modeled as a function of the decompression dose, TR or TR′. An appropriate statistical model for the probability of

occurrence of an event is often assumed to be logistic (6). In terms of a function of dose, the probability P of occurrence of VGE is defined by the logistic regression equation, namely

$$P = \frac{\exp[\beta_0 + \beta_1 (\text{dose})]}{1 + \exp[\beta_0 + \beta_1 (\text{dose})]} \quad (5)$$

where β_0 and β_1 are unknown parameters. The use of a similar probability function for the VGE dose-response relationship, the Hill equation, is documented elsewhere (2, 17, 20). We rewrote *Eq. 5* into a form comparable to the Hill equation

$$P = \frac{[\exp (\text{dose})]^{b_0}}{[\exp (\text{dose})]^{b_0} + {b_1}^{b_0}} \quad (6)$$

where $b_0 = \beta_1$ and $b_1 = \exp(-\beta_0/\beta_1)$ are two statistical parameters. Moreover, unknown physiological parameters, $t_{1/2}$ and P_{other}, also must be optimally determined. The three-parameter model with $P_{other} = 0$ thus becomes a four-parameter model when P_{other} is taken to be a nonzero quantity, and this must be determined so that it maximizes the likelihood function.

Maximum-likelihood method. Maximum-likelihood estimation is the preferred technique (3, 4, 11, 14, 20, 22) to estimate unknown parameters in a model so that the probability function is maximized. Given a set of data, the likelihood function L is defined as the product of the probability densities for the subjects' outcomes

$$L(b_0, b_1) = \prod_{i=1}^{n} (P_i)^{y_i} [1 - (P_i)]^{(1-y_i)} \quad (7)$$

where P_i is the probability and y_i denotes the VGE outcome (1 or 0) for the ith record; total number of records was 426. It is customary to use the natural logarithm of the likelihood function

$$LL(b_0, b_1) = \sum_{i=1}^{n} [y_i \ln (P_i) + (1 - y_i) \ln (1 - P_i)] \quad (8)$$

The log likelihood function, $LL(b_0, b_1)$, is always negative, since $\ln (P_i)$ and $\ln (1 - P_i)$ are negative as P_i lies between 0 and 1. The maximum likelihood estimates of b_0 and b_1 that maximize the LL function can be obtained by solving the following equation

$$\sum_{i=1}^{n} \text{TR}_i (y_i - P_i) = 0 \quad (9)$$

for the 20 different denitrogenation procedures. We used the NONLIN module of SYSTAT version 5.03 (23) to solve *Eq. 9* and to estimate unknown parameters in the models with the sum of absolute values, $|LL|$, minimized by using the quasi-Newton algorithm. In what follows, the absolute value of the LL function will be noted LL. For simplicity, the lowest LL value will be designated as the "best" LL value.

The tissue half time was estimated as part of the model by a trial-and-error method (3, 14) with the use of SYSTAT. The trial-and-error method is comparable with a fully computerized fitting process. A spectrum of half times from 240 to 700 min was tested initially at ~20- to 50-min intervals, and then the half times were progressively decreased to 1-min intervals as the model approached the best fit to the data.

Test of statistical hypotheses. The likelihood ratio test statistic (14, 20) is used to assess whether additional parameters added to a model improve the goodness of fit. The degrees of freedom of a test statistic are equal to the number of parameters estimated in a full model minus the number of parameters in a hypothesized model. The likelihood ratio test statistic is transformed, from a ratio to a difference, by taking twice the difference between the two corresponding LL values. The transformed statistic follows a χ^2 distribution. Finally, a χ^2 table is entered with the calculated likelihood ratio and the difference in degrees of freedom between the two models to determine the appropriate P value.

RESULTS

Table 1 lists the family of models tested, the fitted parameters in each model, and the LL value obtained in each case. The three-parameter model with only N_2 dissolved tissue tension in the expression of dose defined by *Eq. 3* ($P_{other} = 0$), resulted in an LL value of 255.01. The ability to describe the response variable improved by accounting for an additional dissolved gas tissue tension other than N_2 in the dose expression of *Eq. 4*. The four-parameter model ($P_{other} \neq 0$) returned an LL of 251.70, the best LL value that we encountered, indicating that it has the best fit to the data. A decrease of 3.31 LL units by the addition of P_{other} in dose is statistically significant at $P = 0.012$ under the likelihood ratio test. We also define an upper and lower boundary of the LL value (14, 20) to further evaluate the goodness of fit of our best model. The hypothesis that dose of decompression is not useful in predicting VGE defines the "null" model; it is considered as an upper boundary. This is a constant-probability model with one scaling parameter that is estimated by the odds ratio of cases with VGE vs. no VGE. This model returned a value of 290.46 for LL, which significantly differs from all the other models tested. The LL value of 240.08 corresponded to the low-boundary case of the

Table 1. *Models tested*

Model	Parameter(s)	LL
Three and four-parameter models		
Three-parameter model (*Eq. 3*)	$t_{½}$ (420 min), b_0, b_1	255.01
Four-parameter model (*Eq. 4*)	$t_{½}$ (329 min) P_{other} (19.1 kPa), b_0, b_1	251.70
Upper and lower model-boundary cases		
Null model	b_0	290.46
Discontinuous model (multistep)	23 separate b_0 values	240.08

The log likelihood (LL) is expressed in absolute value. Null model is defined with a dose value of zero; therefore, *Eq. 5* becomes

$$P = \frac{e^{b_0}}{1 + e^{b_0}}$$

where parameter b_0 is computed by using the value of probability (P) directly obtained by the odd ratio of observed venous gas emboli (VGE) cases vs. non-VGE cases. In this study, $P = 0.425$. In the case of discontinuous model, P was computed by this odd ratio separately for each group of subjects. P_{other}, additional dissolved gas tissue tension; $t_{½}$, tissue half time for washin and washout of N_2.

Table 2. *Parameter estimates of the best model (with Eq. 4 for the dose)*

Parameter	Estimate	Asymptotic SE	Estimate/SE	Units
P_{other}	19.1	4.64	4.12	kPa
$t_{½}$	329	NA	NA	min
b_0	4.39	0.59	7.44	Dimensionless
b_1	8.12	1.15	7.06	Dimensionless

NA, nonapplicable.

"discontinuous" model, which consisted of separate null models for the 23 groups of data. This discontinuous model, of course, is too data specific to be effective for prediction beyond the range of observations utilized. The discontinuous model and the four-parameter model are, however, not statistically different, since the likelihood ratio test based on the 19 degrees of freedom for the χ^2 statistics yielded a P value >0.50.

Table 2 lists information for the best fit four-parameter model shown in Table 1. The estimated value for P_{other} was 19.1 kPa (143 mmHg). The asymptotic SE for P_{other} was 4.64, which is small, relative to the parameter estimate. The asymptotic correlation matrix in Table 3 indicates that P_{other} was poorly correlated with b_0; therefore, it merits retaining P_{other} in the model (12). However, P_{other} was significantly correlated with b_1, implying that a change in P_{other} would have caused large changes in b_1. The estimates of b_0 and b_1 were several times larger than their SE values, thus indicating their significance in the model. The $t_{1/2}$ had a value of 329 min.

Because $t_{1/2}$ was estimated from trial-and-error modification of potential models, the study of these models allows further insight into relations between $t_{1/2}$ and P_{other}. Close inspection of Fig. 1 shows that the distribution of isopressure isopleths (LL vs. $t_{1/2}$, at six different values of P_{other}) follows a specific pattern. The parabolic shape of these isopleths is a property of the maximum likelihood optimization. As P_{other} increases in value, the isopleth becomes steeper. The minimum on the isopleth corresponds to the best fit of this model with the data. The intercept of the 19.1 isopleth with the 329-min $t_{1/2}$ corresponds to the best fit model. On the other hand, the $t_{1/2}$ estimate for the three-parameter model located at the minimum of the 0 kPa isopleth has a value of 420 min. Figure 1 also shows that our best fit model is robust, since slight variations of P_{other}, e.g., within 2 kPa of 19.1 kPa, hardly affect the LL value. Furthermore, variations of P_{other} within the range of the SE (4.64 kPa) do not significantly affect the estimated model.

Another approach to making comparison between models is the graphic illustration of goodness of fit

Table 3. *Asymptotic correlation matrix of parameter estimates for the best model*

	P_{other}	b_0	b_1
P_{other}	1.000		
b_0	0.0658	1.000	
b_1	0.9844	0.0321	1.000

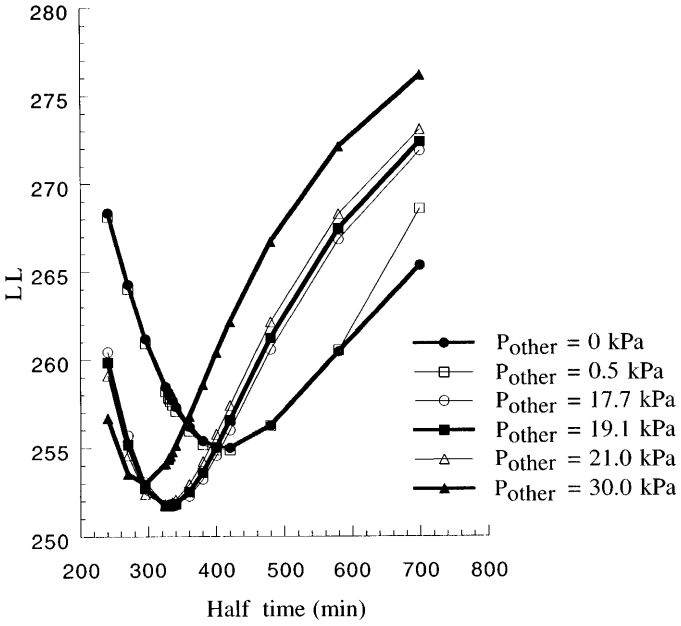

Fig. 1. Plot of six isopressure isopleths on natural logarithm of likelihood function (LL) vs. half time $t_{1/2}$ corresponding to six additional dissolved gas tissue tension (P_{other}) values of 0, 0.5, 17.7, 19.1, 21.0, or 30.0 kPa. Three isopleths, 17.7, 19.1, and 21.0 kPa, are almost superimposed; their LL minima are nearly equal, occurring at the same $t_{1/2}$. Because there is no significant difference among the three cases, the 19.1-kPa isopleth is taken to be the best fit model with the lower LL number. The 17.7-kPa isopleth corresponds to the estimates of mixed venous blood (or tissue) tensions of O_2, CO_2, and water vapor pressure.

as shown in Figs. 2 and 3. Each circle represents a group of subjects, and the size of a circle is proportional to the corresponding group size; there were 23 groups. For a given group, the value on the y-axis is the observed incidence of VGE in this group. The sigmoidal curves show the predicted probability of VGE by two different models: the best fit four-parameter model (Fig. 2) and a three-parameter model (Fig. 3). The models were fitted using a NASA data set consisting of 426 individual observations, as described earlier. The position of all the circles around the curve provides a visual impression of the fit; circles close to the sigmoidal curve indicate a better fit of the model to the data. However, this goodness of fit criterion based on the examination of group incidence is limited because of the lack of reliability of the visual interpretation of observed incidences. Because the model fit takes into account the size of groups of data as weight for each group of subjects, the model represents the larger groups of subjects better than it does the smaller groups. Overall, the best fit model (Fig. 2) does not seem to over- or underpredict the incidence of VGE, except for a few small groups of subjects. In contrast, Fig. 3 depicts a poor fit for the three-parameter model with a 240-min $t_{1/2}$, since it did over- and underestimate the VGE incidence even in larger groups of subjects, and circles are dispersed away from the model curve. Although the model fit is weighted according to the size of subject groups, Fig. 3 shows that a model with an inappropriate $t_{1/2}$ and absence of P_{other} fails to accu-

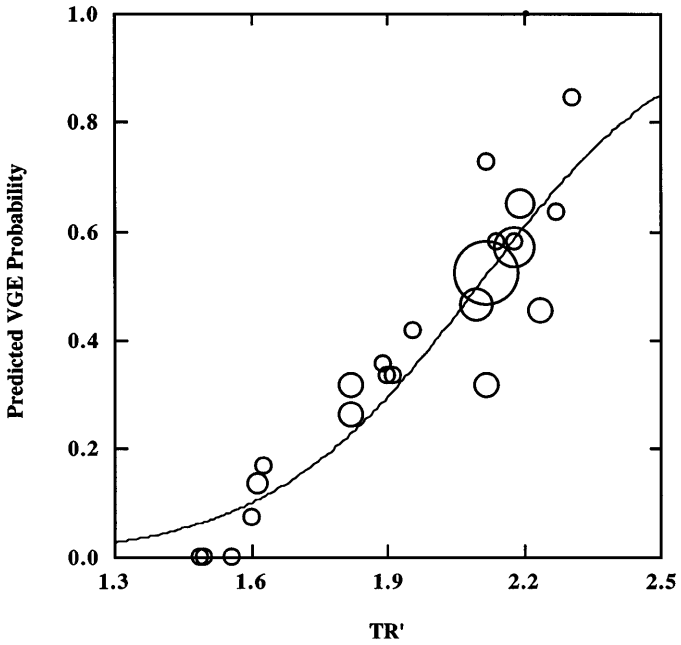

Fig. 2. Display of goodness of fit between our best model and observed incidence in groups of tests composing the data set. Dose is defined as tissue ratio (TR′) from *Eq. 4;* parameter estimates were $t_{1/2}$ = 329 min, and P_{other} = 19.1 kPa. Area of a circle is proportional to no. of subjects in a group; smallest circle has 3 subjects, and largest circle has 59. Estimated probability curve intercepts centers of larger circles (59, 35, and 28 subjects). Three subjects in topmost smallest circle have a venous gas emboli (VGE) incidence of 1; therefore, model underestimates the outcome for this group.

rately predict the observed incidence, even in the case of larger groups of subjects.

Because $P_{A_{N_2}}$ (or Pa_{N_2}) was estimated by using *Eq. 1,* it was appropriate to determine whether variations

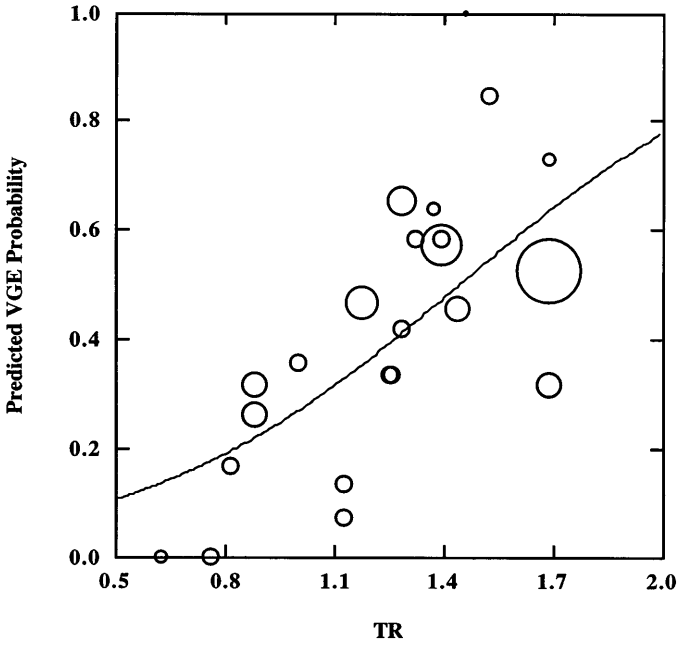

Fig. 3. Display of goodness of fit of a 3-parameter model with $t_{1/2}$ of 240 min; a model with a poor fit to the data (*LL* = 268.35). Dose is defined as TR from *Eq. 3.* Model over- and underpredicts incidence of VGE for all groups of data.

in the respiratory exchange ratio R affect the predictability of the model. We added R as an additional parameter to the four-parameter model and evaluated the model for values of R between 0.70 and 1.0. The ability to describe the response variable is not affected by including R as a parameter. The model is robust, since variations of R between 0.70 and 1.00 do not influence the *LL* value (251.70). Clearly, variations in R and, therefore, small changes in dissolved N_2 tissue fraction have no influence on the model.

DISCUSSION

Presence of Bubbles

We considered only the existence of bubbles and their relationship to pressures of dissolved gases in the model. The model determines the probability of bubble formation on the basis of total tension of dissolved gases in tissue before decompression. However, the accuracy of the Doppler detection is limited. Precordial Doppler detection reflects the quantity of bubbles, but we do not know how to evaluate the sensitivity of the device. Stationary bubbles spawned in the microcirculation cannot be detected by Doppler-shift ultrasonography (7) but may be detectable when dislodged by flexing the limb at the time of Doppler detection (1). A free-gas phase, which is static or of small volume (7) and outside of the limit of sensitivity of the ultrasonic device, can give rise to false negatives (that is, no bubbles are detected, although they are present).

Mechanistic Hypotheses

Tissues with higher dissolved N_2 gas tissue tension than ambient pressure facilitate bubble formation (5, 12). The generation of bubbles from "gas micronuclei" through "nucleation processes" (9, 16) is then followed by an initial explosive bubble-growth phase (12) during the supersaturation. However, our results indicate that dissolved N_2 may not be the only gas to initiate this explosive bubble-growth phase. This explosive growth involves the immediate surroundings of the bubble and may recruit other dissolved gases in the tissue, e.g., CO_2, O_2, water vapor, and even argon (1 kPa). The accelerated log logistic survival model predicted that DCI (and presumably bubbles) may occur when the altitude pressure is ~20 kPa, even though estimated N_2 pressure was zero in the 360-min compartment (3); therefore, this finding suggests a metabolic gas participation in bubble formation. After complete washout of dissolved N_2 in a tissue, the dissolved metabolic gases in the tissue would evolve from solution as ambient pressure approaches a vacuum (3).

The initial explosive-growth phase precipitates a series of events. Bubble size is inversely proportional to surface tension pressure, and the driving force for diffusion of gas into a bubble increases as surface tension pressure diminishes (12). Nitrogen tension in the tissue becomes a driving force for diffusion, causing N_2 to diffuse from tissue to nascent bubble. Once molecules of N_2 are captured inside the newly generated bubble, they are involved in the N_2 partial pres-

sure of the bubble as an outward radial pressure. In contrast, pressure due to surface tension is an inward radial pressure that tends to reduce the bubble volume. Thus, in modeling bubble growth, the surface tension pressure should be subtracted from N_2 dissolved tissue tension. Similarly, tissue elastic recoil is also an inward radial pressure as well as O_2 ambient pressure; both quantities should then be subtracted from the N_2 dissolved tissue tension.

Underlying mechanisms of bubble growth suggest that surface tension pressure and tissue elastic recoil are not involved in P_{other}. If P_{other} is not due to inward radial elastic forces, it should then be caused by gas(es) in physical solution in the tissue before the initial explosive-growth phase. The positive sign of P_{other} unmasks the contribution of an outward radial pressure due to this (these) dissolved gas(es).

Assuming that P_{other} is due to gas(es) previously dissolved in tissues, it is questionable whether the tissue gas(es) tension could follow various distributions with time. Indeed, an alternative to the single-exponential tissue-gas exchange for N_2 and to the constant second-term P_{other} of *Eq. 4* has to be examined. The number of plausible tissue types considered in the analysis may, in fact, be more than one (18). It has been shown (in dogs) that tissue isobaric gas exchange for ^{133}Xe (21) is better described by two or three exponential processes in series. The exponential-series analysis (18) assigns one exponential term or $t_{1/2}$ for inert-gas washout for each tissue present in the expression of dose. These models were applied to predict probability of DCI in diving (11, 22), and it was found that the prediction of DCI incidence was similar for both the series and parallel arrangement of tissues (11). It is questionable how a detailed description of the tissue gas exchange for N_2 including another exponential term in lieu of P_{other} in *Eq. 4* would predict the VGE outcome in the NASA hypobaric exposures. Therefore, we tested (although analysis is not shown) an expression of dose derived from a double-exponential gas exchange in a single tissue or a monoexponential gas exchange in a parallel arrangement of two tissues, each tissue with a different exponential term (22). This dose was then used in the logistic model. The addition of more parameters in the model even further reduced the goodness of fit. In contrast to some DCI data from hyperbaric exposures (11, 22), a monoexponential gas exchange in a single tissue for N_2, as described in our analysis, better fitted the data of hypobaric exposures than a complex gas-exchange kinetics with two exponential terms. The rationale behind these observations is that P_{other} is not an additional pressure due to N_2, which would be disregarded by the $Pti_{N_2}(t)$ term of *Eq. 4*, and that noninert gas(es) would assist N_2 during the initial explosive bubble-growth phase.

Clearly, two types of tissue gas exchange appear in the expression for dose, TR′, in the best fit four-parameter model. Our best predictor for the total driving tension of the tissue ratio is made up of two pressure terms, each with a different relation to time. The two types of tissue gas exchange were *1*) an elimination of dissolved N_2 exponentially related with time, as described by others (5, 18); and *2*) a gas tension in terms of P_{other}, which remains constant, presumably due to metabolic gases. Among all dissolved gases in tissues, this exponential elimination appears to be a characteristic of N_2 tissue gas exchange.

The aforementioned mechanistic premises allow further insight into properties of P_{other} in bubble formation. However, no direct measurement could verify any postulate about P_{other}. Our statistical analysis shows a correlation between P_{other} and the model parameter b_1, and thus a decrease in the *LL* value may be due to an improvement in the model caused by the addition of P_{other} in determining dose.

It is also unclear whether the magnitude for P_{other} obtained in this analysis is a coincidence. The value of 143 mmHg (19.1 kPa) is approximately the tension (BTPS) of metabolic gases in tissue or in mixed venous blood. This finding suggests that nearly all the dissolved gas, other than the N_2 that remains in physical solution in the tissue, has also been utilized to separate the gas phase.

The dissolved tissue tension of all gases involved in the bubble growth, or driving tension, warrants a brief description. Figure 4 shows two dose-response curves of the best fit four-parameter model corresponding to the two altitude pressures of 30 and 45 kPa, respectively. As a result of a complete denitrogenation [$Pti_{N_2}(t) = 0$], the driving tension still available is ~19.1 kPa; P_{other}, presumably because of metabolic gases, remains constant, whereas the dissolved N_2 tissue tension in the expression of dose depends on the denitrogenation procedure. In contrast, without preliminary denitrogenation, and according to our analysis, the total driving tension that can potentially generate bubbles in tissues is 93.3 kPa; it is calculated by subtracting the arteriovenous O_2 difference (8 kPa) from the standard pressure

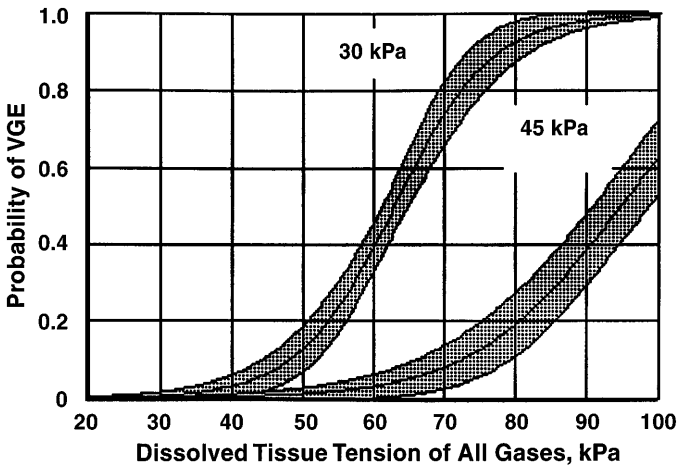

Fig. 4. Probability of VGE predicted by best model as function of dissolved tissue tension of gases generating bubbles. Two isopressure isopleths are displayed for 2 altitude pressures of 30 kPa (*top* curve) and 45 kPa (*bottom* curve). Nonzero probability of VGE starts to rise for a driving pressure of ~20 kPa. At altitude pressure of 30 kPa, without denitrogenation, model predicts occurrence of VGE with probability 1 when a dissolved gas tissue tension is 100 kPa. The 95% confidence interval is shown by shaded area.

(101.3 kPa). The pressure difference of 8 kPa is due to a phenomenon known as the "oxygen window" (15) because metabolism lowers partial O_2 tension in tissues below the value in arterial blood. The 95% confidence intervals were computed based on the propagation of error formula (14). It is seen that the confidence intervals are narrower in the case of 30 kPa than in the case of 45 kPa. The confidence interval provides a range for the parametric values, but it does not establish the accuracy of the estimate. Furthermore, the larger the sample size, the narrower the confidence intervals (3).

Fractions of Gases

The transfer of gases into nascent bubbles is related to their pressures in tissues at the end of the denitrogenation. The washout of dissolved N_2 in tissue depends on the denitrogenation; when excess of dissolved N_2 is removed from the tissue, metabolic gases fraction is obliged to be larger in nascent bubbles (13). The fraction of presumed metabolic gases was calculated for each of the 20 procedures as the ratio of the parameter estimate of P_{other} (equal to 19.1 kPa) to the estimated N_2 dissolved tissue tension at the end of denitrogenation given by *Eq. 2*. The fraction-generating bubbles (for $R = 0.82$) ranged from 21 to 44%, whereas the balance N_2 fraction ranged from 56 to 79%. The latter estimation applies to the initial explosive bubble-growth phase; to estimate the fraction of metabolic gases that diffuse in and out of the bubble, after this initial phase, it is appropriate to use mathematical simulations of gas bubbles (13). Furthermore, during the slower bubble growth, simulations showed that the metabolic gases made up even larger fractions of the bubble because of transients for CO_2 and O_2 (13).

The mechanistic role of metabolic gases in bubble formation appears to be inversely proportional to the excess of dissolved N_2 in tissue; comparison of hypobaric and hyperbaric exposures indicates significant difference. The P_{other} value derived from these NASA hypobaric decompressions is higher than values from direct measurements in diving experiments with guinea pigs breathing air or gas mixtures (8); metabolic gases fraction in bubbles was ~10%, with the balance of 90% due to inert gas. In human dives, there is a slight chance that O_2 could be 40% as effective as N_2 in producing a risk of DCI (19). In hyperbaric conditions, dissolved N_2 tissue tensions and fractions are large, whereas metabolic tissue tensions and fractions remain constant. Therefore, the fraction of inert gas that is likely to participate in the bubble-formation process should be greater in hyperbaric decompression than in hypobaric decompression. Moreover, a detailed model of tissue gas exchange considered in terms of either a series or parallel arrangement of tissues may provide a better fit to the data from diving exposures.

Conclusions

Our statistical analysis of empirical data suggests a significant role of gases other than N_2 in bubble formation. First, the additional parameter of tension P_{other} is attributed to gases that are in physical solution in tissue at the end of the denitrogenation. Second, this tension of dissolved gases remains constant throughout the denitrogenation, whereas N_2 tissue exchange follows an elimination that exponentially decreases with time. An exponential distribution in lieu of the P_{other} term used in *Eq. 4* would have impaired the model prediction. Finally, third, the internal pressure exerted by gases other than N_2 becomes an outward radial pressure of gas(es) in the bubble during the initial explosive-growth phase. It appears that metabolic gases may assist the initial explosive bubble-growth phase, as shown by our analysis.

P. P. Foster performed this research at National Aeronautics and Space Administration (NASA) Johnson Space Center as an External Postdoctoral Fellow of European Space Agency (8–10 rue Mario-Nikis, 75738 Paris cedex 15; associated with Laboratoire de Physiologie de l'Environnement, Faculté de Médecine Lyon Grange-Blanche, 8 Ave. Rockefeller, 69373 Lyon cédex 08, France) and as a visiting scientist through the Universities Space Research Association, Division of Space Life Sciences, 3600 Bay Area Blvd., Houston, TX 77058. Research of R. S. Chhikara was partially supported under NASA Grant NAG-9-802.

Address for reprint requests: P. P. Foster, Life Sciences Research Laboratories, Environmental Physiology Laboratory (SD3), NASA-Lyndon B. Johnson Space Center, Houston, TX 77058.

Received 4 October 1995; accepted in final form November 7, 1997.

REFERENCES

1. **Adams, J. D., R. M. Olson, and G. A. Dixon.** Use of the precordial bubble detector in altitude decompressions. In: *Proc. 1979 Aerospace Med. Assoc. Meeting Washington DC 1979*, p. 260–261.
2. **Conkin, J., B. F. Edwards, J. M. Waligora, and D. J. Horrigan.** Empirical models for use in designing decompression for space operations. *NASA Tech. Memorandum 100456*, 1987.
3. **Conkin, J., K. V. Kumar, M. R. Powell, P. P. Foster, and J. M. Waligora.** A probabilistic model of hypobaric decompression sickness based on 66 chamber tests. *Aviat. Space Environ. Med.* 67: 176–183, 1996.
4. **Gerth, W. A., and R. Vann.** Statistical bubble dynamics algorithms for assessment of altitude decompression sickness incidence. In: *Final Report, Contract No. F-336-90-D-0606, Task 0026, Dept. of Anesthesiology, F. G. Hall Hypo-Hyperbaric Center.* Durham, NC: Duke Univ. Medical Center, 1994, p. 6–29.
5. **Hills, B. A.** Effects of decompression per se on nitrogen elimination. *J. Appl. Physiol.* 45: 916–921, 1978.
6. **Hosmer, D. A., and S. Lemeshow.** Introduction. In: *Applied Logistic Regression*. New York: Wiley Interscience, 1989, p. 6–20.
7. **Kumar, K. V., J. M. Waligora, and M. R. Powell.** Epidemiology of decompression sickness under simulated space extravehicular activities. *Aviat. Space Environ. Med.* 64: 1032–1039, 1993.
8. **Lillo, R. S., M. E. MacCallum, and J. M. Caldwell.** Intravascular bubble composition in guinea pigs: a possible explanation for differences in decompression risk among different gases. *Undersea Biomed. Res.* 19: 375–386, 1992.
9. **Powell, M. R., J. M. Waligora, and K. V. Kumar.** Decompression gas phase formation in simulated null gravity. In: *25th Int. Conf. on Environmental Systems San Diego SAE Technical Paper*, 1995.
10. **Rahn, H., and W. O. Fenn.** *A Graphical Analysis of the Respiratory Gas Exchange. The O_2-CO_2 Diagram*. Washington, DC: Am. Physiol. Soc., 1955.
11. **Tikuisis, P., R. Y. Nishi, and P. K. Weathersby.** Use of the maximum likelihood method in the analysis of chamber air dives. *Undersea Biomed. Res.* 15: 301–313, 1988.
12. **Van Liew, H. D., and M. E. Burkard.** Density of decompression bubbles and competition for gas among bubbles, tissue, and blood. *J. Appl. Physiol.* 75: 2293–2301, 1993.

13. **Van Liew, H. D., and M. E. Burkard.** Simulation of gas bubbles in hypobaric decompressions: roles of O_2, CO_2, and H_2O. *Aviat. Space Environ. Med.* 66: 50–55, 1995.
14. **Van Liew, H. D., J. Conkin, and M. E. Burkard.** Probabilistic model of altitude decompression sickness based on mechanistic premises. *J. Appl. Physiol.* 76: 2726–2734, 1994.
15. **Van Liew, H. D., J. Conkin, and M. E. Burkard.** The oxygen window and decompression bubbles: estimates and significance. *Aviat. Space Environ. Med.* 64: 859–865, 1993.
16. **Vann, R. D.** Exercise and circulation in the formation and growth of bubbles. In: *Supersaturation and Bubble Formation In Fluids and Organisms*, edited by A. O. Brubakk, B. B. Hemmingsen, and G. Sundnes. Trondheim, Norway: Tapir, 1989, p. 235–263.
17. **Vann, R. D.** Likelihood analysis of decompression data using Haldane and bubble growth model. In: *Proc. 9th Int. Symp. on Underwater and Hyperbaric Physiology Undersea and Hyperbaric Medical Society Bethesda MD 1987.* p. 165–181.
18. **Weathersby, P. K., E. E. P. Barnard, L. D. Homer, and K. G. Mendenhall.** Stochastic description of inert gas exchange. *J. Appl. Physiol.* 47: 1263–1269, 1979.
19. **Weathersby, P. K., B. L. Hart, E. T. Flynn, and W. F. Walker.** Role of oxygen in the production of human decompression sickness. *J. Appl. Physiol.* 63: 2380–2387, 1987.
20. **Weathersby, P. K., L. D. Homer, and E. T. Flynn.** On the likelihood of decompression sickness. *J. Appl. Physiol.* 57: 815–825, 1984.
21. **Weathersby, P. K., K. G. Mendenhall, E. E. P. Barnard, L. D. Homer, S. S. Survanshi, and F. Vieras.** Distribution of xenon gas exchange rates in dogs. *J. Appl. Physiol.* 50: 1325–1336, 1981.
22. **Weathersby, P. K., S. S. Survanshi, L. D. Homer, B. L. Hart, R. Y. Nishi, E. T. Flynn, and M. E. Bradley.** *Statistically Based Decompression Tables. I. Analysis of Standard Air Dives: 1950–1970.* Bethesda, MD: Naval Medical Research Institute, 1985, NMRI 85-16.
23. **Wilkinson, L.** *SYSTAT: the System for Statistics.* Evanston, IL: SYSTAT Inc., version 5.03, 1990, p. 342–387.
24. **Wolfram, S.** *MATHEMATICA: A System for Doing Mathematics by Computer.* Champaign, IL: Wolfram Research Inc., version 2.2, 1993.